SUPPLEMENTAL RESULTS

Effect of 50 or 500 μM bumetanide.

We have tried blocking NKCC with a low concentration (50 μM) of bumetanide to rule out the possibility that inactivation of NKCC during Ca^{2+} spiking contributes to the negative E_{gly} shift after Ca^{2+} spiking (n = 5). The resting E_{gly} (in TTX, without dye) shifted by –3.4 ± 1.7 mV (p = 0.012, paired *t*-test) during the initial 15 min of bumetanide superfusion, and then remained relatively stable (ΔE 0–0.6 mV) over the next 15 min. The largest shift (–6.1 mV) in resting E_{gly} was observed from a cell with a control resting E_{gly} of –69.8 mV, the most positive among the 5 cells, and the smallest shift (–1.1 mV) was from a cell with the most negative control E_{gly} (–76.7 mV). The correlation coefficient (*r*) between the control resting E_{gly} and the magnitude of negative shift in resting E_{gly} in bumetanide was –0.88 (n = 5, p = 0.049). Among the four cells in which resting E_{gly} were measured > 10 min after bumetanide wash-out, only the cell that had the largest negative shift in the drug showed a partial recovery (by 2.2 mV) in E_{gly}, and in others the E_{gly} shifted further negative by 0.5 to 1.3 mV. Ca^{2+} spiking still induced a negative shift in E_{gly} in bumetanide of similar magnitude to control conditions in all 5 cells. In 2 of 5 cells, the half-time of recovery from the negative E_{gly} shift appeared delayed by about 5 sec in bumetanide compared to under control conditions, but in other cells the time course was almost identical.

As a final check for our hypothesis, we examined E_{gly} under 500 μM bumetanide. At this concentration, KCCs are expected to be blocked (IC_{50} or K_i for KCCs, 40 ~ 180 μM; Gamba, 2005) in addition to NKCCs, while anion exchangers may not be significantly affected (IC_{50} for AE, 820 μM; Culliford et al. 2003). During initial 12 min of 500 μM bumetanide (in TTX) perfusion, the resting E_{gly} was monitored with cells held at –75 mV in v-clamp, and afterwards the activity-dependent E_{gly} shift was examined. Glycine responses were slightly attenuated in 500 μM bumetanide. The net change in resting E_{gly} after 12 min in bumetanide was either positive or negative (n = 5 cells). The direction of such shifts appeared to depend on the level of control resting E_{gly}. Two cells with the control E_{gly} at ~ – 74 mV showed positive shifts (~ 2 mV) during the first 2–3 min and then the resting E_{gly} shifted negative resulting in < 2 mV net negative shifts at the end of

12 min. Two other cells with the resting E_{gly} at –80 and –85 mV showed 5.8 and 3.5 mV positive shift, respectively, during the initial 3 min, while 10 min later the net shift in E_{gly} was +4.1 mV for both cells. For the remaining cell with the control E_{gly} at –67 mV, the resting E_{gly} shifted only negative (–5.9 mV) during perfusion of 500 μM bumetanide. Except for this cell, the resting E_{gly} was monitored during wash-out of 500 μM bumetanide: the E_{gly} shifted negative for all of them (–1.5 to –9 mV) during > 10 min of wash-out. That the resting E_{gly} shifted positive, although transiently, during 500 μM bumetanide wash-in and that it shifted negative at wash-out are supportive of inhibition of steady-state KCC activity by 500 μM bumetanide. The activity-dependent negative shift in E_{gly} remained in 500 μM bumetanide, and the time-course of recovery was not noticeably different from control condition, as observed with 50 μM bumetanide. For comparison of the magnitude of peak negative shift between the control and 500 μM bumetanide, current injection was increased (by 10–100 pA) in bumetanide to evoke similar number of Ca^{2+} spikes (± 9 spikes) to control condition, as fewer Ca^{2+}spikes were evoked in 500 μM bumetanide. The peak negative E_{gly} shift did not significantly change by 500 μM bumetanide (n = 4, mean ΔE = –0.1 mV, paired *t*-test, p = 0.39).

$[Ca^{2+}]_i$ change associated with weak acid/base application.

Changes in $[Ca^{2+}]_i$ during intracellular acidification or alkalinization induced with weak acid or base have been reported in various cell types, but the direction of change is inconsistent across different studies. For example, increase in $[Ca^{2+}]_i$ was shown during both the intracellular alkalinization and acidification induced by NH_4Cl or other weak base and weak acid by Batlle et al. (1993), Martinez-Zaguilan et al. (1996), OuYang et al. (1994) and Wu et al. (1999), but a decrease in $[Ca^{2+}]_i$ during NH_4Cl-induced intracellular alkalinization has also been demonstrated by Iino et al. (1994) and Kaila and Voipio (1990). We wondered therefore whether in CWCs, the propionate-induced acidification and the TMA-induced alkalinization were associated with a rise and fall in $[Ca^{2+}]_i$, respectively. If true, then both the weak acid-mediated and the complex spiking-mediated negative shift in E_{gly} might be regarded as a consequence of Ca^{2+}'s modulation of Cl^- transporters. We did not monitor $[Ca^{2+}]_i$ during the propionate or TMA challenge but have done simultaneous Fura-2 and SNARF imaging with NH_4Cl on 5 CWCs held at

–75 mV in v-clamp (in TTX). Five mM NH_4Cl for CWCs caused a barely noticeable alkalinization at wash-in, which was soon followed by an acidification during the presence of NH_4Cl (2 min). The peak intracellular acidification occurred within 1 min of NH_4Cl wash out (–15.4 ± 2.8 in %ΔF/F, n = 5). In none of the 5 CWCs, was there a noticeable change in Fura-2 signal ($Ca^{2+}{}_i$) during wash-in and out of NH_4Cl, while an 8-sec complex spiking or Ca^{2+} spiking produced a clear signal (–27.6 ± 4.6 in %ΔF/F) in the same cells. Therefore, considering that the NH_4Cl-induced intracellular acidification is larger than that by propionate (–8.4 ± 3.1 in %ΔF/F), it seemed unlikely that $[Ca^{2+}]_i$ rose significantly during the propionate-induced acidification in CWCs.

The change in the negative E_{gly} shift imposed by nominal removal of HCO_3^-/CO_2.
The degree of negative E_{gly} shift on an intracellular acidification appeared lessened in HEPES/O_2 compared with that in the control, HCO_3^-/CO_2-buffered, condition. This was supported by the following findings: 1) in 5 cases (from 5 cells) of control-HEPES/O_2 pair of E_{gly}/pH_i series with 8-sec depolarization in which the number of evoked Ca^{2+} spikes was similar (0 to 4 more Ca^{2+} spikes in HEPES/O_2), the peak acidification was larger (by 165 ± 22 % in SNARF ΔF/F) in HEPES/O_2 than in control condition (p = 0.002, paired *t*-test) while the magnitude of negative E_{gly} shift was 0.1 ± 0.9 mV less in HEPES/O_2 (p = 0.79, paired *t*-test)(Figure 8Ai). 2) in 8 cases (from 8 cells) of control-HEPES/O_2 pair in which the negative E_{gly} shift was similar in magnitude (0 to 0.4 mV larger in HEPES/O_2), the peak acidification was larger (by 176 ± 22 %) again in HEPES/O_2 than in controls (p < 0.001, paired *t*-test) with 5.8 ± 6.2 more Ca^{2+} spikes evoked in HEPES/O_2 (p = 0.034, paired *t*-test). Also, the time of peak negative E_{gly} shift became delayed to the next measurement point (10 to 15 sec later) in 6 of 12 cells subjected to HEPES/O_2, including 3 cells in which the peak time in control condition was at the first point (2 sec) after spiking (e.g. Fig 8Ai).

SUPPLEMENTAL DISCUSSION

Estimated range of resting $[Cl^-]_i$ and potential causes of slow negative drift in E_{gly}

The relation between $[Cl^-]_i$ and E_{gly} according to the Goldman-Hodgkin-Katz (GHK) voltage equation, $E_{gly} = (RT/F)\ \ln(([Cl^-]_i + r\ [HCO_3^-]_i)/([Cl^-]_o + r\ [HCO_3^-]_o))$, is

illustrated in Figure S3A-B for a range of $[HCO_3^-]_i$, 6–18 mM (corresponding to pH_i 6.78–7.25), with the ratio (*r*) of HCO_3^- permeability (P_{HCO3}) to that of Cl^- (P_{Cl}) of 0.2 (A) or 0.1 (B) (P_{HCO3}/P_{Cl} for glycine receptors has been measured to be 0.11 (Bormann et al., 1987) or 0.4 (Fatima-Shad and Barry, 1993). The pH_i indicated for each curve of different $[HCO_3^-]_i$ in Figure S3 is derived from $[HCO_3^-]_i/[HCO_3^-]_o = 10^{(pHi-pHo)}$ at fixed pH_o = 7.30 and $[HCO_3^-]_o$ = 20 mM, based on the assumption that the partial pressure, solubility, and the dissociation constant of CO_2 is equal intra- and extracellularly (Roos and Boron, 1981). Over an arbitrary resting pH_i of 6.95 – 7.15, the possible E_{gly} at $[Cl^-]_i$ of 4 mM is –84.4 ~ –80.2 mV (Δ 4.2 mV) and that at $[Cl^-]_i$ of 12 mM –61.5 ~ –59.6 mV (Δ 1.9 mV). Using the same range of resting pH_i and the two extreme values of the measured resting E_{gly}, –58 and –87 mV, the range of resting $[Cl^-]_i$ among CWCs was 2–14 mM.

The actual range of $[Cl^-]_i$ among different CWCs may be wider than that estimated above because of the tendency for the resting E_{gly} to drift negative with time, and the reported resting E_{gly} values are those obtained some time after the drift had been noticed. The reason for the slow negative drift over time in resting E_{gly} is not clear. It is possible that, during the gramicidin perforated-patch recording, activation of KCCs and/or inactivation of NKCC (lowering $[Cl^-]_i$) occurred or an intracellular acidification (lowering $[HCO_3^-]_i$) developed. Slow intracellular acidification may occur unrelated to the perforated-patch recording due to possible build-up of metabolically generated acids in slice (cf. Trapp et al., 1996); however, this is unlikely in our case given that the negative drift in E_{gly} is generally faster during the early period of recording. The more negative resting E_{gly} in AM dye-loaded cells may be associated with lower resting pH_i levels due to increased intracellular acid generation from the de-esterification reaction, the byproducts of which are acetic acid and formaldehyde (which can be converted to formic acid) (Spray et al., 1984; Tsien and Pozzan, 1989). However, the acid build-up from AM ester hydrolysis is not expected to be too large because acetic acid and formaldehyde can diffuse out of the cell, and acetate may also be eliminated from the cell along with H^+ by

monocarboxylate transporters (Pierre and Pellerin, 2005).

E_{gly} shifts viewed with the Goldman-Hodgkin-Katz equation

A typical change in E_{gly} and pH_i associated with complex/Ca^{2+} spiking and simple spiking is drawn in Figure S3D with labeled E_{gly} points. The change in $[Cl^-]_i$ involved in the activity-dependent shifts in E_{gly} was estimated by identifying points along the curves of E_{gly} vs. $[Cl^-]_i$ at different pH_i levels (P_{HCO3}/P_{Cl} = 0.2; Fig. S3A). The finding from such examination is described below with labels in parentheses referring to Figure S3D. 1) The decrease in $[Cl^-]_i$ that can occur with a negative shift in E_{gly} associated with a pH_i decrease (P→Q or P→R) is less than, i.e. limited by, what would occur without a pH_i change. This leads to the prediction of less than 1.6 mM and 0.7 mM decrease in $[Cl^-]_i$ for a 3 mV negative shift accompanied with a pH_i decrease from E_{gly} –60 mV and –80 mV, respectively. The $[Cl^-]_i$ decreases less the larger the intracellular acidification for a given magnitude of negative E_{gly} shift. 2) For a negative E_{gly} shift associated with a pH_i decrease (P→Q) and for a positive E_{gly} shift occurring with a pH_i increase (R→S), it is possible for the $[Cl^-]_i$ to change in the opposite direction to that of pH_i if the pH_i change is large enough. For example, if pH_i = 7.15 ($[HCO_3^-]_i$ = 14 mM) and E_{gly} = –72 mV ($[Cl^-]_i$ = 6.5 mM) in the baseline condition and the E_{gly} shifts by –1 mV (i.e. P→Q), then $[Cl^-]_i$ must *rise* if the pH_i falls more than 0.06 unit ($\Delta[HCO_3^-]_i$ = –1.7 mM). If the E_{gly} shifts by –3 mV (to –75 mV), the $[Cl^-]_i$ rises for acidification > 0.20 pH unit ($\Delta[HCO_3^-]_i$ = –5.0 mM). 3) However if the E_{gly} goes negative with a pH_i rise (Q→R) or shifts positive with a pH_i drop (P□→Q□), the $[Cl^-]_i$ will fall (Q→R) or rise (P□→Q□), and the change in $[Cl^-]_i$ is greater than that without a pH_i change. For example, if the E_{gly} and pH_i at baseline is –72 mV and 7.15, respectively, and each shifts by +1 mV and –0.04 after simple spiking (P□→Q□), the increase in $[Cl^-]_i$ is 0.56 mM, which is 0.2 mM larger than what is expected without a pH_i change.

The predictions of the effect of pH_i decrease (i.e. lowered $[HCO_3^-]_i$) on the E_{gly} shifts were based on a P_{HCO3}/P_{Cl} of 0.2 for the glycine receptor. The influence of $[HCO_3^-]_i$ on

the magnitude of E_{gly} shifts becomes less if the P_{HCO3}/P_{Cl} is smaller (Fig. S3B) or if the concentration of intracellular and extracellular HCO_3^- is low at the same P_{HCO3}/P_{Cl} (Fig. S3C). It should be added that the P_{CO2} and pH_o may not be constant during the spiking activity associated with E_{gly} shifts (Chesler 2003; Voipio and Kaila, 1993), which would compromise our estimations of $[Cl^-]_i$ change based on constant values of P_{CO2}, pH_o, and $[HCO_3^-]_o$.

We do not know the absolute values of resting pH_i or the magnitude of pH_i decrease induced by complex/Ca^{2+} spiking in CWCs. However, 20 mM propionate caused a similar range of peak changes in SNARF signal (–5 ~ –12 % ΔF/F) to that observed with complex/Ca^{2+} spiking in CWCs; moreover, intracellular acidifications of 0.04–0.15 pH unit were observed with 20 mM propionate in other cell types in HCO_3^--buffered condition (Saarikoski et al., 1997; Xiong et al., 2000; Jacobs et al., 2008). Thus, assuming CWCs buffer pH at a level similar to that of other cells, the peak decrease in pH_i with complex/Ca^{2+} spiking may have been less than 0.2 pH units in HCO_3^--buffered condition. Therefore, at least for cases where the peak negative E_{gly} shifts of > 3 mV occurred after some recovery from peak acidification (e.g. Fig 5Bi control, 280 pA trace), the $[Cl^-]_i$ must have fallen below baseline level, probably by 1~2 mM. Given that the predicted decrease in $[Cl^-]_i$ was generally less than 2 mM with up to 4 mV negative shift in E_{gly}, it is understandable that the increase in MQAE fluorescence (reflecting a decrease in $[Cl^-]_i$) was weak and became noticeable after rather excessive induction of complex spiking in each cell tested (Fig 6Bii); a ~1 mM change in $[Cl^-]_i$ seems unlikely to yield a detectable change in MQAE signal based on the intracellular calibration curve of Marandi et al. (2000).

Factors contributing to resting E_{gly} in CWCs

Given the discussion above, it is clear that in individual cells, the levels of $[Cl^-]_i$ and $[HCO_3^-]_i$ together determine the E_{gly}. The $[HCO_3^-]_i$ will vary depending on the resting pH_i, the reported value of which ranges 6.90–7.30 in mean and 0.05–0.30 pH units in standard deviation in various rodent neurons (Pocock and Richards, 1992; Ou-yang et al., 1993; Schwiening and Boron, 1994; Leniger et al., 2004). On the

other hand, $[Cl^-]_i$ must be determined by the differing prevalence in expression or activity of inward [e.g. NKCC1 (Plotkin et al., 1997), AE3 (Kopito et al., 1989; Hentschke et al., 2006)] and outward [e.g. KCC2 (Payne et al., 1996; Kanaka et al., 2001), NDCBE (Grichtchenko et al., 2001; Chen et al., 2008)] Cl^- transporters, which might vary in different CWCs. The expression of AE3 or NKCC1 in CWCs is not known at present, but KCC2 protein has been detected in rat DCN (Vale et al., 2005). The mechanism determining the resting E_{gly} in CWCs was not the focus of the present study, but some hints were gathered from the change in resting E_{gly} observed with certain experimental conditions. NKCC1 is likely to provide a steady inward transport of Cl^- in CWCs as 50 μM bumetanide (Supplemental Results) shifted the resting E_{gly} negative. Additionally, AE-mediate Cl^- influx may contribute to steady-state $[Cl^-]_i$ considering that H_2DIDS or AZA addition (both in HCO_3^-/CO_2-buffered and HCO_3^-/CO_2-free Ringer) shifted the resting E_{gly} negative. However, this alternatively could arise from the lowered $[HCO_3^-]_i$ associated with a possible decrease in resting pH_i secondary to block of constitutively active Na^+-HCO_3^- co-transport. In some cells, the H_2DIDS or AZA/HEPES/O_2-induced negative shift in resting E_{gly} involved conversion to a hyperpolarizing glycine response (e.g. Fig 7A). This suggests that the resting Cl^- extrusion mechanism partially survived in H_2DIDS, and thus is most likely due to KCC. The initial positive shift and the variability of the net shift in the resting E_{gly} observed in 500 μM bumetanide (Supplemental Results) suggests that the balance between the activities of NKCC and KCC sets the level of resting E_{gly} in CWCs.

The net transport direction of the electroneutral Cl^--HCO_3^- exchange by AE is determined by the transmembrane concentration gradient of Cl^- and HCO_3^- (equilibrium when $[Cl^-]_i/[Cl^-]_o = [HCO_3^-]_i/[HCO_3^-]_o$), and thus it can be made to work in the reverse mode (Cl^- efflux and HCO_3^- influx) if bath Cl^- is lowered or the intracellular pH_i is decreased enough (Vaughan-Jones, 1986). In our experimental setting of $[Cl^-]_o$ = 136.8 mM, $[HCO_3^-]_o$ = 20 mM and pH_o = 7.30, the reversal pH_i for AE's transport direction seems to be very low (e.g. 6.24 if $[Cl^-]_i$ = 12 mM, 5.94 if $[Cl^-]_i$ = 6 mM), thus AE is expected to transport Cl^- inward under most conditions.

However, while AE's participation in maintenance of high $[Cl^-]_i$ has been suggested in some smooth muscle cells (Chipperfield and Harper, 2000) and in cardiac Purkinje fibers (Vaughan-Jones, 1986), whether AE can provide significant Cl^- influx at the resting pH_i (6.90–7.30) in neurons is not yet known. The Cl^--HCO_3^- exchange activity in several non-neuronal cell types as well as in AE2- or AE3-transfected cell lines has been shown to be rather low at baseline pH_i increasing steeply at alkaline pH_i (> ~ 7.2) (Olsnes et al., 1986; Boyarsky et al., 1988; Lee et al., 1991; Jiang et al., 1994; Leem et al., 1999). Considering that the Cl^- influx by AE is accompanied by gain of acid equivalents, mechanisms removing acid, such as Na^+-H^+ exchangers (NHEs) or Na^+-HCO_3^- co-transporters (NBCs), may need to work in concert with AE for it to contribute to intracellular Cl^- level without disturbing the resting pH_i (Vaughan-Jones, 1986).

References

Batlle DC, Peces R, LaPointe MS, Ye M, Daugirdas JT (1993) Cytosolic free calcium regulation in response to acute changes in intracellular pH in vascular smooth muscle. Am J Physiol Cell Physiol 264:C932-943.

Boyarsky G, Ganz MB, Sterzel RB, Boron WF (1988) pH regulation in single glomerular mesangial cells. II. Na+-dependent and -independent Cl(-)-HCO3- exchangers. Am J Physiol 255:C857-869.

Chen LM, Kelly ML, Parker MD, Bouyer P, Gill HS, Felie JM, Davis BA, Boron WF (2008) Expression and localization of Na-driven Cl-HCO(3)(-) exchanger (SLC4A8) in rodent CNS. Neuroscience 153:162-174.

Chesler M, Rice ME (1991) Extracellular alkaline-acid pH shifts evoked by iontophoresis of glutamate and aspartate in turtle cerebellum. Neuroscience 41:257-267.

Chipperfield AR, Harper AA (2000) Chloride in smooth muscle. Prog Biophys Mol Biol 74:175-221.

Culliford SJ, Ellory JC, Lang H-J, Englert H, Staines HM, Wilkins RJ (2003) Specificity of Classical and Putative Cl - Transport Inhibitors on Membrane Transport Pathways in Human Erythrocytes. Cellular Physiology and Biochemistry 13:181-188.

Farrant M, Kaila K (2007) The cellular, molecular and ionic basis of GABA(A) receptor signalling. Prog Brain Res 160:59-87.

Gamba G (2005) Molecular physiology and pathophysiology of electroneutral cation-chloride cotransporters. Physiol Rev 85:423-493

Grichtchenko II, Choi I, Zhong X, Bray-Ward P, Russell JM, Boron WF (2001) Cloning, Characterization, and Chromosomal Mapping of a Human Electroneutral Na+-driven Cl-HCO3 Exchanger. J Biol Chem 276:8358-8363.

Hentschke M, Wiemann M, Hentschke S, Kurth I, Hermans-Borgmeyer I, Seidenbecher T, Jentsch TJ, Gal A, Hubner CA (2006) Mice with a targeted disruption of the Cl-/HCO3-exchanger AE3 display a reduced seizure threshold. Mol Cell Biol 26:182-191.

Iino S, Hayashi H, Saito H, Tokuno H, Tomita T (1994) Effects of intracellular pH on calcium currents and intracellular calcium ions in the smooth muscle of rabbit portal vein. Exp Physiol 79:669-680.

Jacobs S, Ruusuvuori E, Sipila ST, Haapanen A, Damkier HH, Kurth I, Hentschke M, Schweizer M, Rudhard Y, Laatikainen LM, Tyynela J, Praetorius J, Voipio J, Hubner CA (2008) Mice with targeted Slc4a10 gene disruption have small brain ventricles and show reduced neuronal excitability. Proc Natl Acad Sci U S A 105:311-316.

Jiang L, Stuart-Tilley A, Parkash J, Alper SL (1994) pHi and serum regulate AE2-mediated Cl-/HCO3- exchange in CHOP cells of defined transient transfection status. Am J Physiol 267:C845-856.

Kaila K, Voipio J (1990) Dependence of intracellular free calcium and tension on membrane potential and intracellular pH in single crayfish muscle fibres. Pflugers Archiv European Journal of Physiology 416:501-511.

Kanaka C, Ohno K, Okabe A, Kuriyama K, Itoh T, Fukuda A, Sato K (2001) The differential expression patterns of messenger RNAs encoding K-Cl cotransporters (KCC1,2) and Na-K-2Cl cotransporter (NKCC1) in the rat nervous system. Neuroscience 104:933-946.

Kopito RR, Lee BS, Simmons DM, Lindsey AE, Morgans CW, Schneider K (1989) Regulation of intracellular pH by a neuronal homolog of the erythrocyte anion exchanger. Cell 59:927-937.

Lee BS, Gunn RB, Kopito RR (1991) Functional differences among nonerythroid anion exchangers expressed in a transfected human cell line. J Biol Chem 266:11448-11454.

Leem CH, Lagadic-Gossmann D, Vaughan-Jones RD (1999) Characterization of intracellular pH regulation in the guinea-pig ventricular myocyte. J Physiol 517 (Pt 1):159-180.

Leniger T, Thone J, Bonnet U, Hufnagel A, Bingmann D, Wiemann M (2004) Levetiracetam inhibits Na+-dependent Cl-/HCO3- exchange of adult hippocampal CA3 neurons from guinea-pigs. Br J Pharmacol 142:1073-1080.

Marandi N, Konnerth A, Garaschuk O (2002) Two-photon chloride imaging in neurons of brain slices. Pflugers Arch 445:357-365.

Martinez-Zaguilan R, Gurule MW, Lynch RM (1996) Simultaneous measurement of intracellular pH and Ca2+ in insulin-secreting cells by spectral imaging microscopy. Am J Physiol 270:C1438-1446.

Olsnes S, Tonnessen TI, Sandvig K (1986) pH-regulated anion antiport in nucleated mammalian cells. J Cell Biol 102:967-971.

OuYang YB, Mellergard P, Kristian T, Kristianova V, Siesjo BK (1994) Influence of acid-base changes on the intracellular calcium concentration of neurons in primary culture. Exp Brain Res 101:265-271.

Ou-yang Y, Mellergard P, Siesjo BK (1993) Regulation of intracellular pH in single rat cortical neurons in vitro: a microspectrofluorometric study. J Cereb Blood Flow Metab 13:827-840.

Payne JA, Stevenson TJ, Donaldson LF (1996) Molecular characterization of a putative K-Cl cotransporter in rat brain. A neuronal-specific isoform. J Biol Chem 271:16245-16252.

Pierre K, Pellerin L (2005) Monocarboxylate transporters in the central nervous system: distribution, regulation and function. J Neurochem 94:1-14.

Plotkin MD, Kaplan MR, Peterson LN, Gullans SR, Hebert SC, Delpire E (1997) Expression of the Na(+)-K(+)-2Cl- cotransporter BSC2 in the nervous system. Am J Physiol 272:C173-183.

Pocock G, Richards CD (1992) Hydrogen Ion Regulation in Rat Cerebellar Granule Cells Studied by Single-Cell Fluorescence Microscopy. Eur J Neurosci 4:136-143.

Romero MF, Fulton CM, Boron WF (2004) The SLC4 family of HCO 3 - transporters. Pflugers Arch 447:495-509.

Saarikoski J, Ruusuvuori E, Koskelainen A, Donner K (1997) Regulation of intracellular pH in salamander retinal rods. J Physiol 498:61-72.

Schwiening CJ, Boron WF (1994) Regulation of intracellular pH in pyramidal neurones from the rat hippocampus by Na(+)-dependent Cl(-)-HCO3- exchange. J Physiol 475:59-67.

Spray D, Nerbonne J, Campos de Carvalho A, Harris A, Bennett M (1984) Substituted benzyl acetates: a new class of compounds that reduce gap junctional conductance by cytoplasmic acidification. J Cell Biol 99:174-179.
Trapp S, Luckermann M, Brooks PA, Ballanyi K (1996) Acidosis of rat dorsal vagal neurons in situ during spontaneous and evoked activity. J Physiol 496:695-710.
Tsien R, Pozzan T (1989) Measurement of cytosolic free Ca2+ with quin2. Methods Enzymol 172:230-262.
Vale C, Caminos E, Martinez-Galan JR, Juiz JM (2005) Expression and developmental regulation of the K+-Cl- cotransporter KCC2 in the cochlear nucleus. Hear Res 206:107-115.
Vaughan-Jones RD (1986) An investigation of chloride-bicarbonate exchange in the sheep cardiac Purkinje fibre. J Physiol 379:377-406.
Voipio J, Kaila K (1993) Interstitial PCO2 and pH in rat hippocampal slices measured by means of a novel fast CO2/H(+)-sensitive microelectrode based on a PVC-gelled membrane. Pflugers Arch 423:193-201.
Wu M-L, Chen J-H, Chen W-H, Chen Y-J, Chu K-C (1999) Novel role of the Ca2+-ATPase in NMDA-induced intracellular acidification. Am J Physiol Cell Physiol 277:C717-727.
Xiong Z-Q, Saggau P, Stringer JL (2000) Activity-Dependent Intracellular Acidification Correlates with the Duration of Seizure Activity. J Neurosci 20:1290-1296.

SUPPLEMENTAL FIGURE LEGENDS

Figure S1. Measurement of E_{gly} with a voltage ramp protocol
(A-C) An example from one cell illustrating how a series of E_{gly} measurements was made to generate the time plot of E_{gly} with respect to Ca^{2+} spiking. Bath solution contained TTX 0.4 µM, APV 100 µM, and DNQX 10 µM. (A) The recording began at t = 0 (sec) in i-clamp with a bias current for setting the V_m close to –75 mV. In this cell, the V_m was held below –75 mV with –30 pA bias to reduce the post-Ca^{2+} spiking depolarization. At t = 5 and every 15 sec (except just after Ca^{2+} spiking) the recording mode was switched to v-clamp for 4 sec to measure E_{gly} with the voltage ramp protocol (B). Ca^{2+} spiking was induced for 8 sec at t = 35 in i-clamp. The short V_m traces from different time points show responses to 2 mM-8 msec glycine puffs. (Bi left) The unit voltage ramp command protocol was run 4 times consecutively to obtain 2 glycine responses (1st and 3rd run) and 2 control responses. (Bi, right) Ramp responses obtained 5 sec before Ca^{2+} spiking, 8 sec after Ca^{2+} spiking, and at the end of the series. A trace without glycine (gray) and one with glycine (red) are superimposed. The uncorrected E_{gly} was taken from the voltage on the ramp where the two responses crossed. (Bii) I-V plot of glycine currents at different times with respect to Ca^{2+} spiking was generated by subtracting the control ramp response from that with glycine in each set of ramp responses. (C) Time plot of R_s-corrected E_{gly}. Gray rectangle shows the period of Ca^{2+} spiking. The clamp current at V_H= –75 mV, I_{hold}, is also plotted below each E_{gly} points. Inward shift in I_{hold} after Ca^{2+} spiking reflects depolarized V_m, as shown in t=58 trace in (A).
(D) Slow negative drift in the resting E_{gly} in CWCs. E_{gly} was measured in TTX, DNQX and APV with the voltage ramp protocol. (Di) Each series of symbols represents measurements from one cell, and 24 cells are shown. Symbols are connected with a dotted line if one or more Ca^{2+}spike experiment as in (A-C) was run in between. The first point in each series is the first E_{gly} with R_s < 60 MΩ. The last point in a series is the last measurement either before recording termination or before a drug was added. (Dii)

Plot of difference in the resting E_{gly} between the last measurement and the first measurement versus the time elapsed between the two measurements. Dots represent single CWCs, and are from 94 cells including the cells shown in (Di).

Figure S2. Activity-induced intracellular acidifications detected with fluorescent imaging (A) The SNARF fluorescence images and intensity signals at acquisition. Excitation at 547 nm, emission filtered at > 600 nm. A CWC was loaded with SNARF-5F by diffusion of the AM form of dye from the recording pipette. In each image shown in the top row, the ROIs are placed inside the cell body, over the recording pipette on the right of cell body, and in the background. The fluorescence in the recording pipette is from the intracellular compartment evaginated into the pipette tip. (Ai, bottom) The average fluorescent intensity of the 3 ROIs (top) as appeared in the image acquisition software during an 8-s challenge protocol. A 150-pA current injection evoked complex spikes during the period indicated with thick bar. (Aii bottom) An example showing the detection of patch rupture from an abrupt fall in the fluorescence of the ROI drawn over the recording pipette.
(B) pH imaging performed with a different indicator, pHrodo (A gift from Daniel Beecham, Molecular Probes/Invitrogen). This rhodamine-based dye (excited at 555 nm, emission filtered at > 600 nm) increases fluorescence as pH decreases. In both (Bi) and (Bii) the image and the bottom pH trace are from one cell, and the top trace is from a different cell. (Bi) pHrodo loaded into a CWC through perforated patch with 50 μM of the AM form in a recording solution composed of (in mM) 147 K-gluconate, 4 NaCl, 4 NaOH, 10 HEPES. The nearby area was stained by the dye leaking from the recording pipette when the cell was patched. The acidification on complex spiking induced with an 8-sec current injection occurred in the same pattern as that seen with SNARF. (Bii) pH imaging in whole-cell configuration was done using the free acid form of pHrodo (100 μM) in a K-gluconate-based recording solution containing 9 mM HEPES and nucleotides (pH 7.30). 8-sec current injections evoking complex spikes induced an acidification, but unlike with perforated patch recording, the acidification decayed faster and was followed by apparent rebound alkalinization and acidification.

Figure S3. Plots of E_{gly} vs. $[Cl^-]_i$ according to the Goldman-Hodgkin-Katz equation.
(A-B) Each curve represents the relation between $[Cl^-]_i$ and E_{gly} according to the Goldman-Hodgkin-Katz voltage equation with the P_{HCO3}/P_{Cl} at 0.2 (A) or 0.1 (B) for the glycine receptor at a given $[HCO_3^-]_i$ ranging 6–18 mM. The pH_i indicated is derived from $[HCO_3^-]_i/[HCO_3^-]_o = 10^{(pHi-pHo)}$ at fixed pH_o = 7.30 and $[HCO_3^-]_o$ = 20 mM, based on the assumption that the partial pressure, solubility, and the dissociation constant of CO_2 is equal intra- and extracellularly. The plot of E_{Cl} is also drawn according to the Nernst equation. The temperature used in equations is 34 °C.
(C) The curves were generated as in (A) but with 3 mM $[HCO_3^-]_o$ in equilibrium with 7.2 mmHg CO_2 at pH_o 7.20, a potential condition of slices in nominally HCO_3^-/CO_2-free Ringer. The value of P_{CO2} was derive from the assumed 1% endogenous CO_2 taken from Lamsa and Kaila (1997), and the pH_o was set lower than that of the HCO_3^-/CO_2-free Ringer, 7.30, as observed in other preparations (e.g. Chesler and

Rice, 1991; Voipio and Ballanyi, 1997).
(D) Schematic of typical time-dependent change in average V_m, E_{gly}, pH_i associated with an 8-sec complex/Ca^{2+} spiking (Di) and simple spiking (Dii).

References

Chesler M, Rice ME (1991) Extracellular alkaline-acid pH shifts evoked by iontophoresis of glutamate and aspartate in turtle cerebellum. Neuroscience 41:257-267.

Lamsa K, Kaila K (1997) Ionic Mechanisms of Spontaneous GABAergic Events in Rat Hippocampal Slices Exposed to 4-Aminopyridine. J Neurophysiol 78:2582-2591.

Voipio J, Ballanyi K (1997) Interstitial PCO2 and pH, and their role as chemostimulants in the isolated respiratory network of neonatal rats. J Physiol 499:527-542.

Figure S1

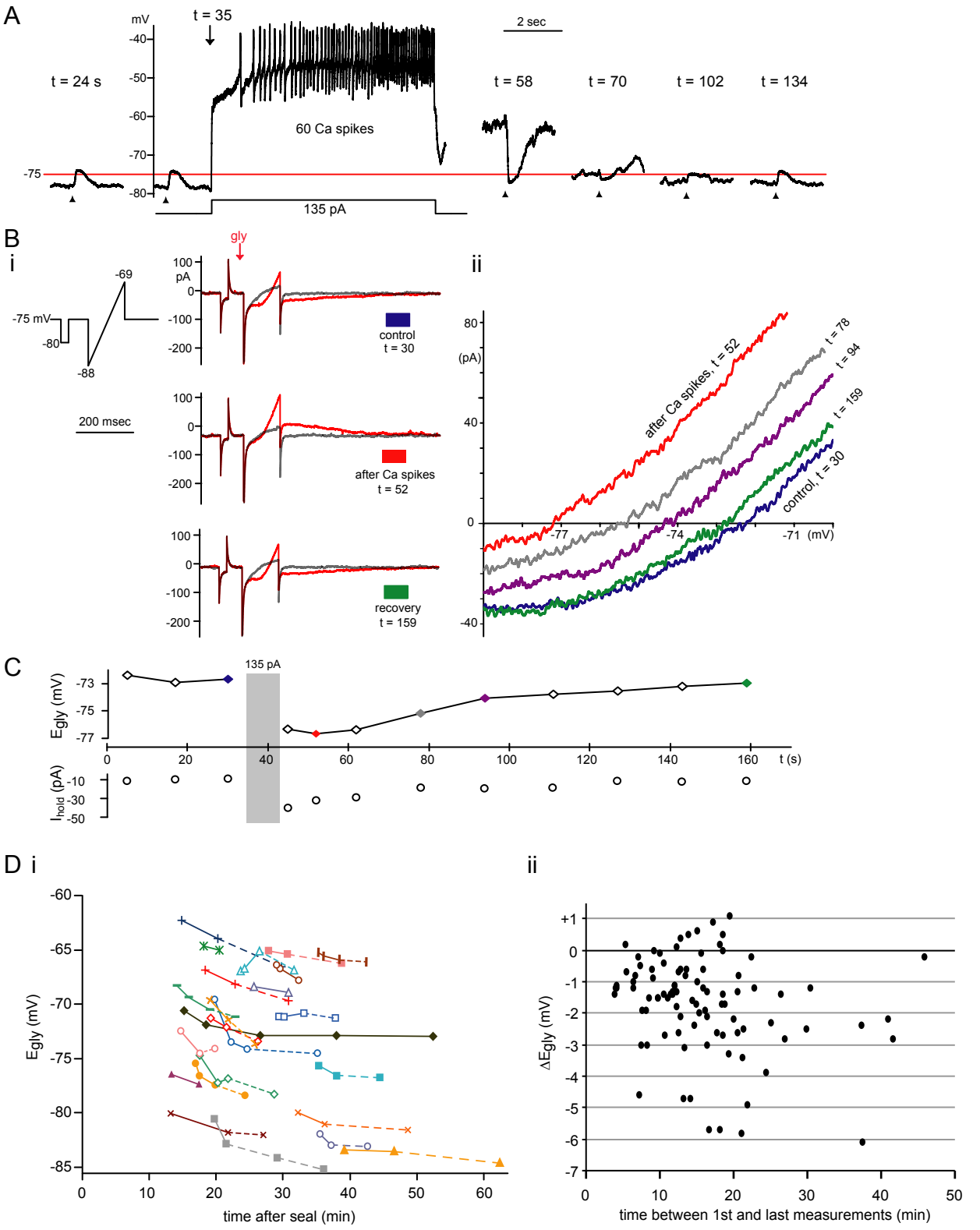
A
mV
t = 35
2 sec
t = 24 s
-40
-50
-60
-70
-75
-80
60 Ca spikes
t = 58
t = 70
t = 102
t = 134
135 pA
B
i
gly
-69
-75 mV
-80
-88
200 msec
100
pA
0
-100
-200
control
t = 30
after Ca spikes
t = 52
recovery
t = 159
ii
80
(pA)
40
0
-40
-77
-74
-71 (mV)
after Ca spikes, t = 52
t = 78
t = 94
t = 159
control, t = 30
C
135 pA
Egly (mV)
-73
-75
-77
0
20
40
60
80
100
120
140
160
t (s)
Ihold (pA)
-10
-30
-50
D i
Egly (mV)
-60
-65
-70
-75
-80
-85
0
10
20
30
40
50
60
time after seal (min)
ii
ΔEgly (mV)
+1
0
-1
-2
-3
-4
-5
-6
-7
0
10
20
30
40
50
time between 1st and last measurements (min)

Figure S2

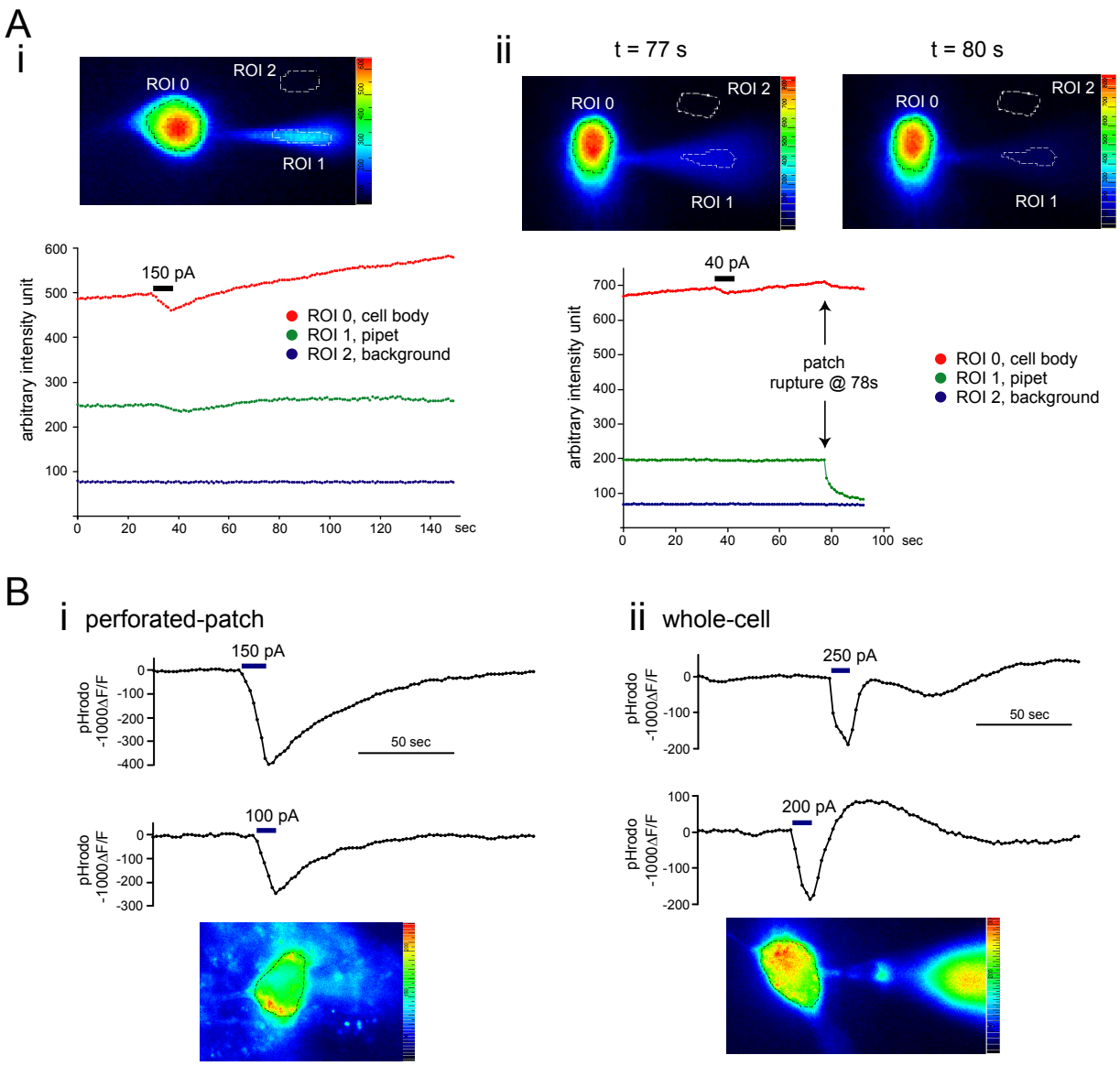
A
i
ROI 0
ROI 2
ROI 1
150 pA
arbitrary intensity unit
ROI 0, cell body
ROI 1, pipet
ROI 2, background
sec
ii
t = 77 s
t = 80 s
40 pA
patch
rupture @ 78s
B
i perforated-patch
150 pA
100 pA
pHrodo
-1000ΔF/F
50 sec
ii whole-cell
250 pA
200 pA

Figure S3

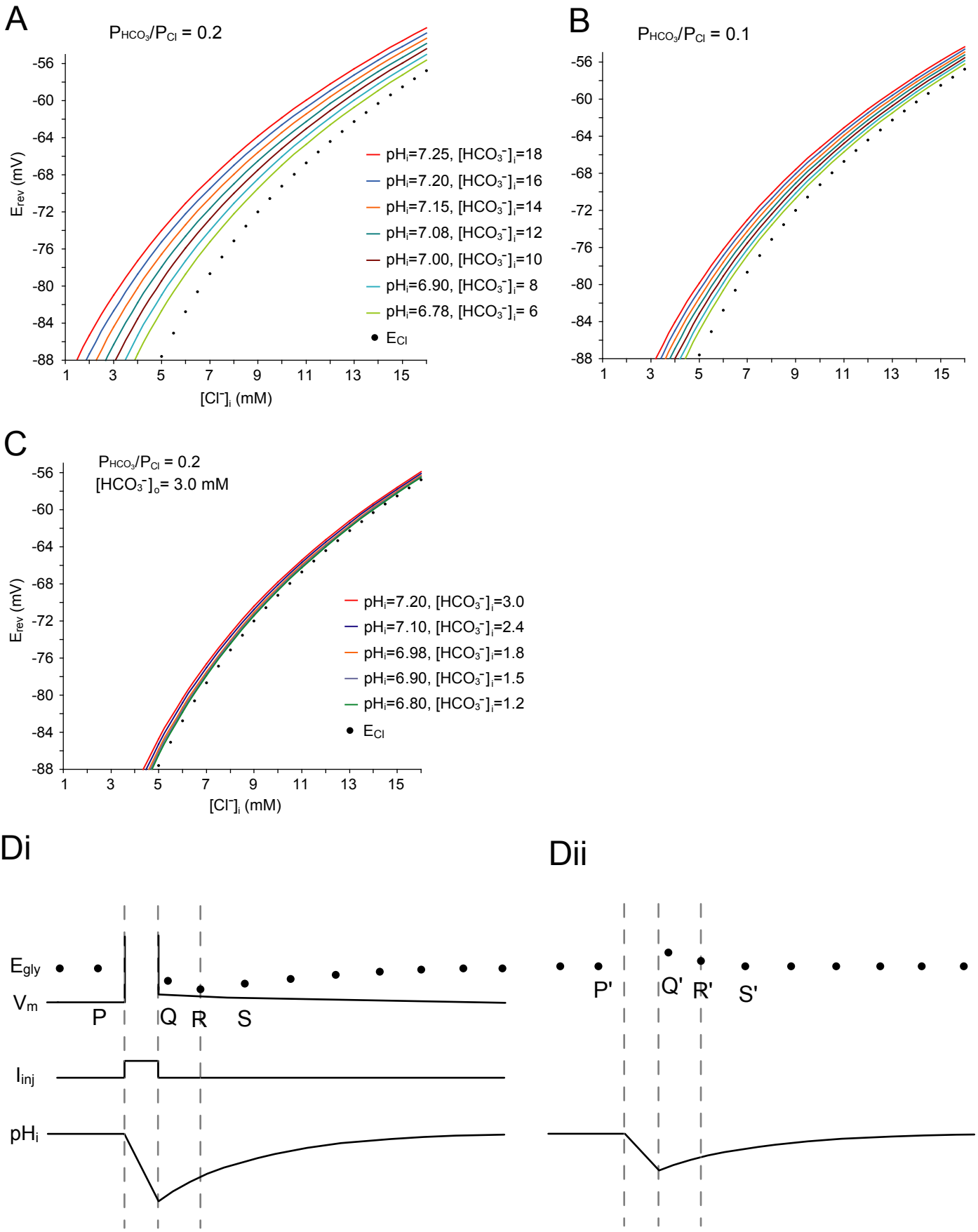
A
P_{HCO_3}/P_{Cl} = 0.2
E_{rev} (mV)
$[Cl^-]_i$ (mM)
pH$_i$=7.25, [HCO_3^-]$_i$=18
pH$_i$=7.20, [HCO_3^-]$_i$=16
pH$_i$=7.15, [HCO_3^-]$_i$=14
pH$_i$=7.08, [HCO_3^-]$_i$=12
pH$_i$=7.00, [HCO_3^-]$_i$=10
pH$_i$=6.90, [HCO_3^-]$_i$= 8
pH$_i$=6.78, [HCO_3^-]$_i$= 6
E_{Cl}
B
P_{HCO_3}/P_{Cl} = 0.1
C
P_{HCO_3}/P_{Cl} = 0.2
[HCO_3^-]$_o$= 3.0 mM
pH$_i$=7.20, [HCO_3^-]$_i$=3.0
pH$_i$=7.10, [HCO_3^-]$_i$=2.4
pH$_i$=6.98, [HCO_3^-]$_i$=1.8
pH$_i$=6.90, [HCO_3^-]$_i$=1.5
pH$_i$=6.80, [HCO_3^-]$_i$=1.2
Di
Dii
E_{gly}
V_m
I_{inj}
pH$_i$
P
Q
R
S
P'
Q'
R'
S'